17th World Conference on Earthquake Engineering, 17WCEE
Sendai, Japan - September 13th to 18th 2020

A NUMERICAL STUDY ON INTERACTION BETWEEN STRUCTURE AND FOUNDATION ROCK DURING EARTHQUAKE USING 3D FEM

W. Hotta[(1)], H. Sonobe[(2)], S. Suzuki[(3)] and M. Hori[(4)]

[(1)] *Manager, Taisei Corporation, ht-wtr00@pub.taisei.co.jp*
[(2)] *Assistant, Taisei Corporation, snbhda00@pub.taisei.co.jp*
[(3)] *Manager, Taisei Corporation, shun1@ce.taisei.co.jp*
[(4)] *Director-General, Japan Agency for Marine-Earth Science and Technology, horimune@jamstec.go.jp*

Abstract

In the seismic evaluation of nuclear power plants, it is necessary to make more accurate numerical computation of the responses of the structures for more reliable stability analysis of built-in facilities and devices. To achieve such computation, we are developing a high performance computing finite element method (HPC-FEM) which can solve models of more than one million degree-of-freedom. A major application of HCP-FEM is the evaluation of seismic responses which are induced by extremely strong ground motion; the responses include contact and separation between the structure and the foundation ground. Numerical analysis often produces high frequency pulses if an analysis model of coarse mesh size is used and joint elements are used at the interface.

In this paper, we develop a contact surface element as an alternative of a joint element, which can more accurately analyze distribution of displacement gap on the contact surface, to accurately analyze the contact and separation. Implementing the contact surface element into HPC-FEM, we carried out numerical experiments of a nuclear power plant building subjected to large ground motion. The responses that were computed by using the joint element and the contact surface element were compared. It was shown that the distribution of vertical stress on the interface were smoother for the contact surface element. Since the contact surface element is more complicated, it is expected that the computational cost becomes larger. However, it was shown in the numerical experiment that the computational cost was slightly smaller for the contact surface element because of faster convergence of the numerical solution. These results indicated potential usefulness of the contact surface element which was implemented into HPC-FEM.

Keywords: contact surface element, high performance computing, large scale numerical model, soil-structure interaction effects, rocking and pounding

1. Introduction

Recently, we began to utilize three-dimensional finite element method (FEM) models in the seismic evaluation of large-scale important structures. The models are alternative of mass spring models or two-dimensional models when more accurate and reliable evaluation is needed. As for structures which contain precise equipments such as pressure vessels, it is necessary to most accurately compute the seismic responses that are induced by strong ground motion, because the responses are used to analyze the stability of the built-in equipments during quakes. Precise computation of the structural seismic response needs a model of high fidelity for both the structure and the foundation ground, to take soil-structure interaction into full consideration. Nevertheless, numerical analysis of three-dimensional FEM is more frequently performed in seismic designs. Analysis models of higher fidelity, which have larger degree-of-freedom, require longer computation time and larger computation memory. Therefore, we are developing a high performance computing finite element method (HPC-FEM) [1-3] that can make a scalable execution of three-dimensional non-linear seismic response analyses of high fidelity models.

A challenge in developing HPC-FEM is to accurately evaluate complicated soil-structure interactions such as rocking and pounding. Extremely strong ground motion causes separation and contact on the interface between the structure and the ground, which inevitably induces responses of higher frequency components with shorter wavelength. HPC-FEM is surely needed to analyze such responses, because high frequency pulses which considerably influence the equipments cannot be accurately analyzed without using finer finite elements and shorter time steps. It should be mentioned that non-linearity inherent to separation and contact requires a larger number of iteration to reach a numerically converged solution. Therefore, high scalability is essential for HPC-FEM.

For the analysis of separation and contact, a joint element proposed by Goodman *et al*. [4, 5] is used as a standard practice. This element is practically useful, because of simple discretization of gap (or displacement discontinuity) on the interface. However, the simple discretization results in a drawback that it cannot accurately analyze the gap behavior. Schellekens *et al*. [6, 7] proposed an interface element based on the detailed processing of discontinuous displacement functions on the contact surface. They pointed out that in quasi-static states traction oscillations occurred near the boundary between the contact and separation areas and that the oscillations could be reduced or diminished by employing Newton cotes or lumped integrals instead of Gauss integral in creating element stiffness matrix. The most appropriate way to reduce the traction oscillations is to geometrically distinguish the contact and separation areas on the interface, by applying suitable remeshing techniques [8, 9]. However, this method is not realistic from the viewpoint of computational costs. As for a model of high fidelity, it needs considerable amount of computation to change the nodes and elements on the interface according to the contact and separation state that changes every time step.

In this study, we propose a new element, called a contact surface element, as an alternative of a joint element. We rigorously formulate this element to account for distribution of gap on the interface. The contact surface element is implemented into HPC-FEM. We need to examine the increase in computational costs due to the implementation, because the contact surface element is more complicated than the joint element and longer iteration is inevitably required in analyzing the non-linear behavior that is inherent to contact and separation.

This paper is organized as follows. First, we preset the contact surface element. While the joint element calculates the nodal force directly from the difference in the displacement of the two nodes facing on the interface, the contact surface element calculates the element stiffness matrix by rigorously considering the spatial distribution of gap on the interface. Next, we verify the contact surface element, analyzing a simple analysis model with HPC-FEM to which the contact surface element is implemented. Finally, we carry out numerical experiments of the seismic response analysis of a nuclear power plant building. The responses that are computed by using the joint element and the contact surface element are compared.

Discussions are made on the potential usefulness of the contact surface element implemented into HPC-FEM, in accurately analyzing contact and separation which are induced by extremely strong ground motion.

It should be pointed out that as a platform for FEM, we employ E-FrontISTR which Taisei Corporation and other five Japanese organizations have been developing. E-FrontISTR is an extension program which is aimed at seismic analysis of civil engineering and building structures; the original program is FrontISTR [10], an open source large-scale parallel FEM program. This platform has a parallel high-speed solver that is based on the conjugate gradient (CG) method with domain decomposition techniques.

2. Concept of contact surface element

We preset the formulation of a four-node contact surface element. In the three-dimensional Cartesian coordinates, denoted by $\boldsymbol{x}$, as shown in Fig. 1, we consider two contact surfaces and introduce the following function of two-dimensional isoparametric coordinates, $\boldsymbol{\xi} = [\xi, \eta]^T$:

$$\boldsymbol{x}(\boldsymbol{\xi}) = \sum_{\alpha=1}^{4} N^{\alpha}(\boldsymbol{\xi})\boldsymbol{x}^{\alpha}, \tag{1}$$

where $\boldsymbol{x}^{\alpha}$ is the coordinates of the α-th node and N^{α} is the shape function. The unit vectors, denoted by $\boldsymbol{s}_{\xi}$ and $\boldsymbol{s}_{\xi}$, are defined on the contact surface, as

$$\boldsymbol{s}_{\xi} = \frac{\frac{\partial \boldsymbol{x}}{\partial \xi}}{\left|\frac{\partial \boldsymbol{x}}{\partial \xi}\right|}, \tag{2}$$

$$\boldsymbol{s}_{\eta} = \frac{\frac{\partial \boldsymbol{x}}{\partial \eta}}{\left|\frac{\partial \boldsymbol{x}}{\partial \eta}\right|}. \tag{3}$$

The unit vector in the normal direction to the contact surface, denoted by $\boldsymbol{n}$, is expressed in terms of $\boldsymbol{s}_{\xi}$ and $\boldsymbol{s}_{\xi}$ as

$$\boldsymbol{n} = \frac{\boldsymbol{s}_{\xi} \times \boldsymbol{s}_{\eta}}{|\boldsymbol{s}_{\xi} \times \boldsymbol{s}_{\eta}|}. \tag{4}$$

Here, × represents the vector product.

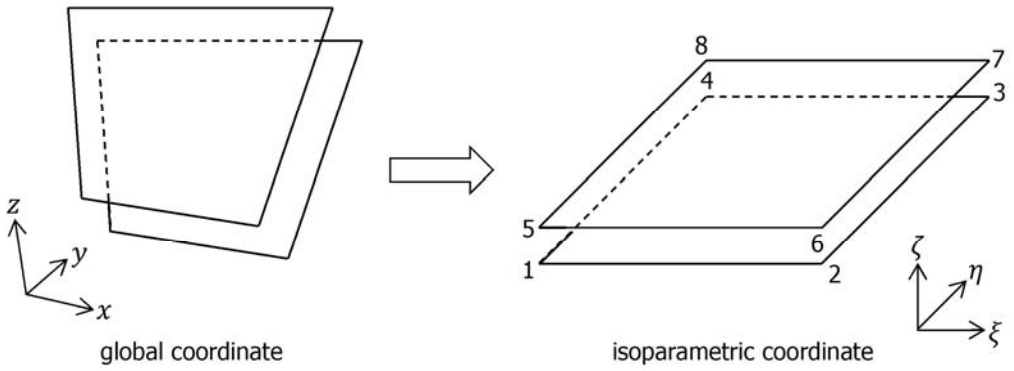

Fig. 1 – Global coordinates and isoparametric coordinates

The vertical and shear spring coefficients on the contact surface are denoted by k_n and k_s, respectively. It is assumed that the springs are uniformly distributed on the interface. Hence, the strain energy stored in the two distributed springs, denoted by U, is computed as

$$U[\Delta \boldsymbol{u}] = \int \frac{1}{2} \Delta \boldsymbol{u} \cdot \left\{ k_n (\boldsymbol{n} \otimes \boldsymbol{n}) + k_s \left(\boldsymbol{s}_\xi \otimes \boldsymbol{s}_\xi + \boldsymbol{s}_\eta \otimes \boldsymbol{s}_\eta \right) \right\} \cdot \Delta \boldsymbol{u} \, \mathrm{d}S_{\boldsymbol{x}}, \tag{5}$$

where $\cdot$ is the inner product, $\otimes$ is the tensor product, and subscript $\boldsymbol{x}$ for $\mathrm{d}S_{\boldsymbol{x}}$ emphasizes that the integration is made with respect to $\boldsymbol{x}$. Note that U is a functional for the function of gap on the contact surface, $\Delta \boldsymbol{u}$ ($\Delta \boldsymbol{u} = \boldsymbol{u}^+ - \boldsymbol{u}^-$ when the displacement above or below the contact surface is denoted by $\boldsymbol{u}^+$ or $\boldsymbol{u}^-$, respectively). The variation of the functional $U[\Delta \boldsymbol{u}]$ is readily computed as

$$\delta U = \int \delta \Delta \boldsymbol{u} \cdot \left\{ k_n (\boldsymbol{n} \otimes \boldsymbol{n}) + k_s \left(\boldsymbol{s}_\xi \otimes \boldsymbol{s}_\xi + \boldsymbol{s}_\eta \otimes \boldsymbol{s}_\eta \right) \right\} \cdot \Delta \boldsymbol{u} \, \mathrm{d}S_{\boldsymbol{x}}. \tag{6}$$

Using the shape function in Eq. (1), we discretize $\Delta \boldsymbol{u}$, as

$$\Delta \boldsymbol{u}(\boldsymbol{\xi}) = \sum_{\alpha=1}^{4} N^\alpha(\boldsymbol{\xi}) \Delta \boldsymbol{u}^\alpha. \tag{7}$$

The element stiffness matrix is computed in carrying out the surface integration in the isoparametric coordinate system, i.e.,

$$K_{ij}^{\alpha\beta} = \left\{ k_n (n_i n_j) + k_s \left(s_{\xi i} s_{\xi j} + s_{\eta i} s_{\eta j} \right) \right\} \int N^\alpha N^\beta J \mathrm{d}S_{\boldsymbol{\xi}}. \tag{8}$$

Here, the superscript is the node number, the subscript is the component in the three-dimensional Cartesian coordinate system, J is the Jacobian, and subscript $\boldsymbol{\xi}$ of $\mathrm{d}S_{\boldsymbol{\xi}}$ emphasizes that the integration is made in the two-dimensional coordinate system $\boldsymbol{\xi}$. As can be seen from Eq. (8), the nodal forces of the contact surface element are calculated from the integral of the forces that are distributed on the contact surface. It should be recalled that the joint element [4, 5] calculates the nodal forces directly from the nodal gap.

The linear equation of the gap and the spring force on the contact surface, denoted by $\Delta \boldsymbol{u}$ and $\boldsymbol{t}$, needs to be changed to a non-linear equation, in order to deal with contact and separation behavior. We employ the following non-linear equation for $\Delta \boldsymbol{u}$ and $\boldsymbol{t}$:

$$\boldsymbol{t} = \begin{cases} \left\{ k_n (\boldsymbol{n} \otimes \boldsymbol{n}) + k_s \left(\boldsymbol{s}_\xi \otimes \boldsymbol{s}_\xi + \boldsymbol{s}_\eta \otimes \boldsymbol{s}_\eta \right) \right\} \cdot \Delta \boldsymbol{u} & \Delta \boldsymbol{u} \cdot \boldsymbol{n} < 0, \\ \boldsymbol{0} & else. \end{cases} \tag{9}$$

According to this equation, the integration $\int N^\alpha N^\beta J \mathrm{d}S_{\boldsymbol{\xi}}$ in Eq. (8) should be performed only on the part of the contact surface that satisfies $\Delta \boldsymbol{u} \cdot \boldsymbol{n} < 0$.

For the integration in calculating element stiffness matrix, higher-order Gauss integral is used when the contact surface element is partially separated. Note that for the linear spring, the Gauss integral is used, the order of which is set according to the order of the shape function. In the case of the nonlinear spring, the gap that is discretized using the shape function generates more complex distribution of the spring forces. The spring force is calculated using Eq. (9), and the Gauss integration points are properly placed on the contact surface. In terms of Gauss integration points and weights, denoted by $\boldsymbol{\xi}^G$ and w^G, the integral in Eq. (8) is expressed as

$$\int N^\alpha N^\beta J \mathrm{d}S_{\boldsymbol{\xi}} = \sum_G N^\alpha(\boldsymbol{\xi}^G) N^\beta(\boldsymbol{\xi}^G) J(\boldsymbol{\xi}^G) w^G. \tag{10}$$

On the right side of Eq. (10), increasing the order of Gauss integral results in the increase in the number of Gauss integration points, but only $\boldsymbol{\xi}^G$ that satisfies $\Delta \boldsymbol{u}(\boldsymbol{\xi}^G) \cdot \boldsymbol{n} < 0$ needs to be included in the summation.

Figure 2 shows the constitutive relations of the contact surface element; in this figure, the negative normal stress is compression. The relation between the vertical gap and normal stress is an indicator of contact and separation. We introduce tensile strength to the non-linear spring; when the normal stress reaches the strength, it becomes zero. The relation between the shear gap and shear stress is more complicated. When not separated, the relation is similar to an elastic-perfect-plastic model, with Mohr-Coulomb equation being adopted for the yield function, denoted by f, i.e.,

$$f(\boldsymbol{\sigma}) = \tau_s - \tau_{yield}, \quad \tau_s = \sqrt{\tau_{s1}^2 + \tau_{s2}^2}, \quad \tau_{yield} = C - \mu\sigma_n, \tag{11}$$

where, τ_s, τ_{yield}, C and μ are the combined shear stress, shear strength, cohesion and friction coefficient, respectively.

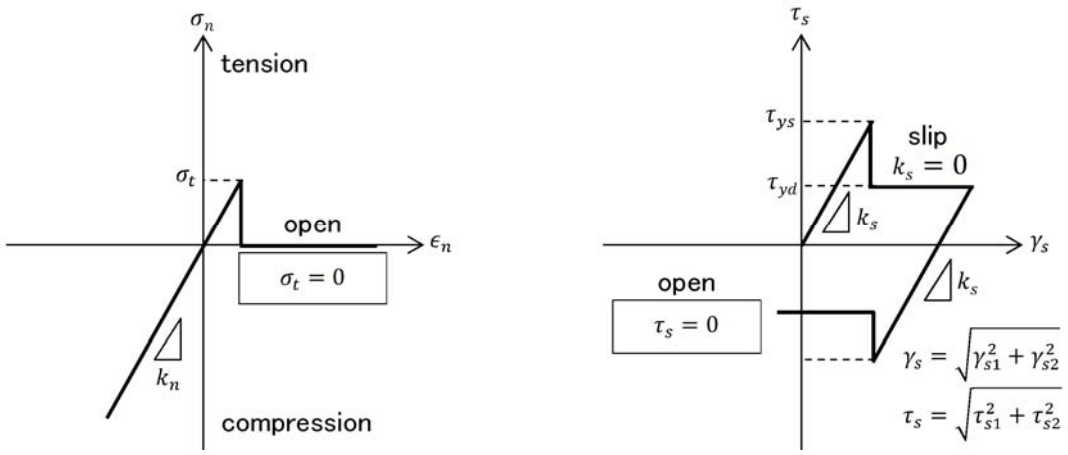

Fig. 2 – Constitutive relations used for contact surface element

Damping coefficient which evaluates the relationship between slip velocity and force is a most important parameter for dynamic state problems. We use the damping matrix for the contact surface element of the following form:

$$C_{ij}^{\alpha\beta} = \{c_n(n_i n_j) + c_s(s_{\xi i} s_{\xi j} + s_{\eta i} s_{\eta j})\} \int N^\alpha N^\beta J \mathrm{d}S_\xi, \tag{12}$$

$$c_n = \frac{h_n}{\pi f_0} k_n, \tag{13}$$

$$c_s = \frac{h_s}{\pi f_0} k_s. \tag{14}$$

Here h_n and h_s are the vertical and shear damping constants, respectively, and f_0 is the natural frequency that is determined by the initial stiffness. Equation (10) is applied in calculating the integral $\int N^\alpha N^\beta J \mathrm{d}S_\xi$ in Eq. (12).

3. Verification of contact surface element

In this section, we verify the proposed contact surface element using a simple analysis model. Figure 3 illustrates the analysis model that is used for the verification. The material properties of concrete and ground are shown in Table 1; linear materials are used, since the main objective of the analysis model is to verify the contact surface element. Table 2 presents the spring constants of the contact surface element. k_n and k_s; these springs are non-linear because they have to represent separation and contact. The number of Gauss integration points on the contact surface is changed, in order to accurately compute the distribution of contact forces. At all the integration points, evaluated is whether the point is in contact or separation.

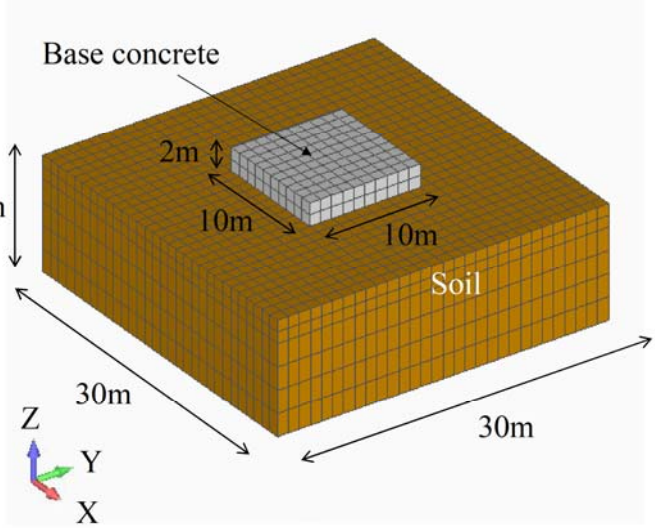

Fig. 3 – Analysis model used for verification

Table 1 – Material properties of concrete and soil used in numerical experiments

	Young Modulus	**Poisson's Ratio**	**Density**
	***E* (kPa)**	***v***	**ρ (t/m^3)**
Concrete	45,490,000	0.3000	2.4
Soil	1,330,000	0.3333	2.0

Table 2 – Deformation characteristic parameters of contact surface used in numerical experiments

Vertical spring coefficient	**Shear spring coefficient**	**Cohesion**	**Friction coefficient**	**Tension stress**
k_n (kN/m/m^2)	**k_s (kN/m/m^2)**	***C* (kN/m^2)**	**μ**	**σ_t (kN/m^2)**
Parametric study	Parametric study	0.00	0.60	0.00

Prior to the dynamic analysis, we performed an initial stress analysis in order to set the initial loading conditions on the contact surface. Figure 4 shows the distribution of vertical stress at the Gauss integration points on the contact surface after the initial stress analysis. The spring coefficients, k_n and k_s, of the contact surface elements were changed in addition to the number of Gauss integration points. When the spring coefficients were $k_n = k_s = 1 \times 10^9$ kN/m/m^2 and the number of Gauss integration points was 16 or 36, separation was observed partially, and the vertical stress tended to oscillate as the number of the Gauss integration points increased from 16 to 36. According to Schellekens *et al.* [6, 7], it is one idea not to use an excessively large spring coefficient for the direction normal to the contact surface. As shown in Fig. 4, when the spring coefficients were $k_n = k_s = 5 \times 10^6$ kN/m/m^2, the non-smooth distribution of vertical stresses was reduced.

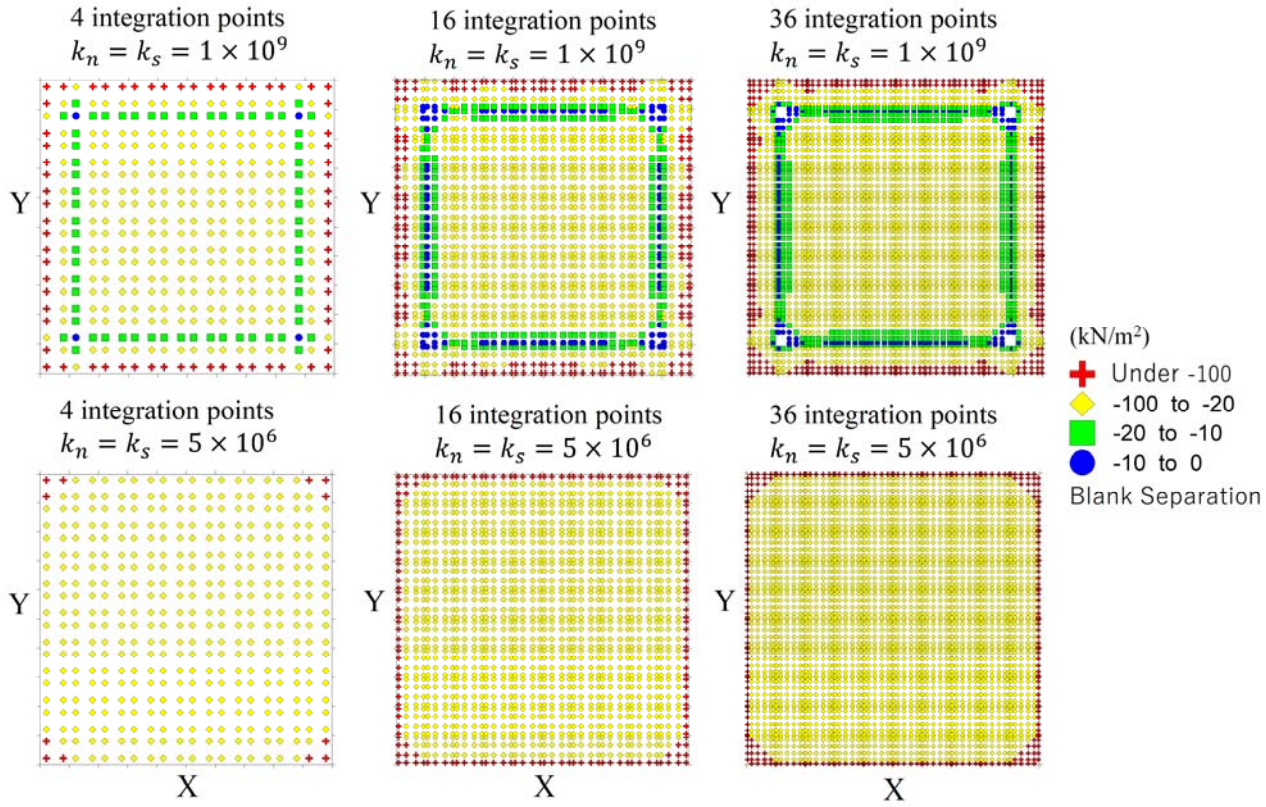

Fig. 4 – Distribution of vertical stress at Gauss integration points on contact surface element after initial stress analysis

We executed the seismic response analysis after the initial stress analysis. According to the Rayleigh damping factor formulation, the coefficients of the mass matrix and stiffness matrix for the Rayleigh damping were set as $\alpha = 1.473$ and $\beta = 0.00127$. $\alpha = 0$ and $\beta = 0.0001$ were set to the contact surface element. For the boundary condition, the bottom of the soil was fixed, and 1.5 times the spectrum waves proposed by Kato *et al*. [11] were used simultaneously in the three directions. The input ground motion is shown in Fig. 5. The time increment was 0.001 sec, and the total number of computation steps was 22,090.

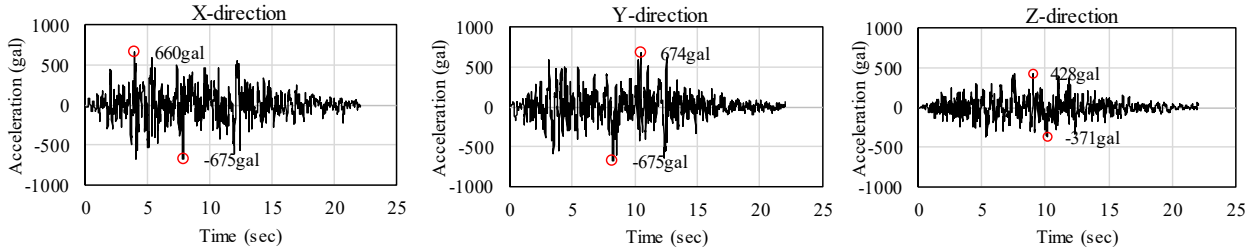

Fig. 5 – Input ground motion

Figure 6 shows the distribution of normal stress on the contact surface at the time of 5.42 sec when the contact area between the foundation and soil was minimized. If the spring coefficient was too large, the stress was affected by the initial stress analysis and the stress distribution was non-smooth even during the

dynamic analysis. However, if the spring coefficient was not so large, the distribution of normal stress on the contact surface became much more smooth. As the number of Gauss integration points increased, the separation area became more stringent. In general, as the elements become finer, the analysis becomes more accurate. The same trend was seen as for the number of Gauss integration points. Near the boundary between the contact and separation areas, there were no noticeable oscillations of vertical stress. This might be the effect of Rayleigh damping which served as numerical damping. It should be noted that how to set appropriate damping coefficients for the contact surface element is not clarified yet.

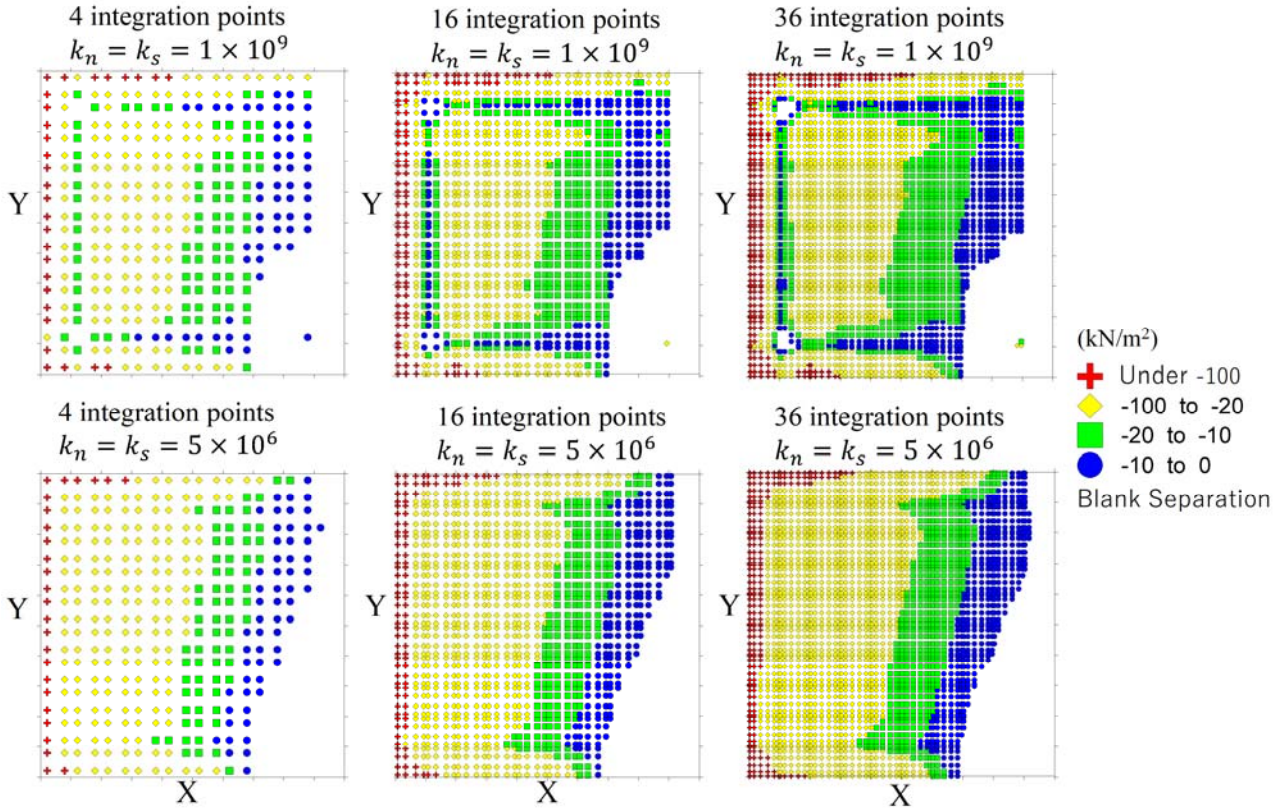

Fig. 6 – Distribution of vertical stress at Gauss integration points on contact surface element during dynamic analysis

Figure 7 shows the total number of iterations for the CG method during the dynamic analysis and the vertical gap between the upperside node and downside node on the contact surface which share the same node in the initial state. This figure shows that setting excessive spring coefficients increases the number of iterations. On the other hand, when small spring coefficients are used, the vertical gap becomes slightly negative, which is regarded as unrealistic phenomena. However, accepting negative vertical gap to some extent results in shortening of numerical computation time as well as suppressing surface force oscillations.

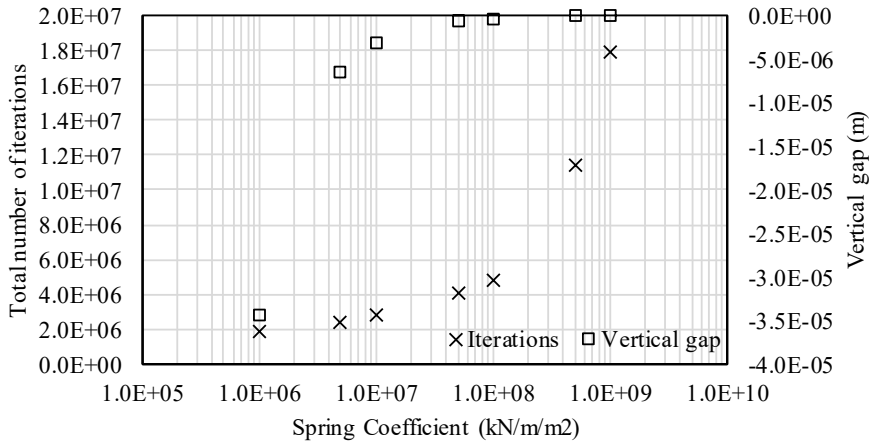

Fig. 7 – Number of iterations for CG method during dynamic analysis and vertical gap after initial stress analysis for different values of spring coefficients

4. Analyses using a high-fidelity analysis model considering soil-structure interaction

4.1 Program settings

We carried out seismic response analyses using HPC-FEM to which the proposed contact surface element was implemented and a three-dimensional high-fidelity model with over 1 million degrees of freedom. The model is shown in Fig. 8, which corresponds to a standard model of U.S. Department of Energy to evaluate the effect of the dynamic interaction between the reactor building and the soil. The reactor building was a hybrid structural model in which solid and shell elements were used for concrete and reinforcement parts, respectively. The material properties of concrete and soil were the same as used in the preceding section, and the spring coefficients of the contact surface were $k_n = k_s = 5 \times 10^6$ kN/m/m^2. For the comparison, we made an analysis model which employed the standard joint element instead of the contact surface element. The contact surface and joint element were set at the interface between the building and the ground.

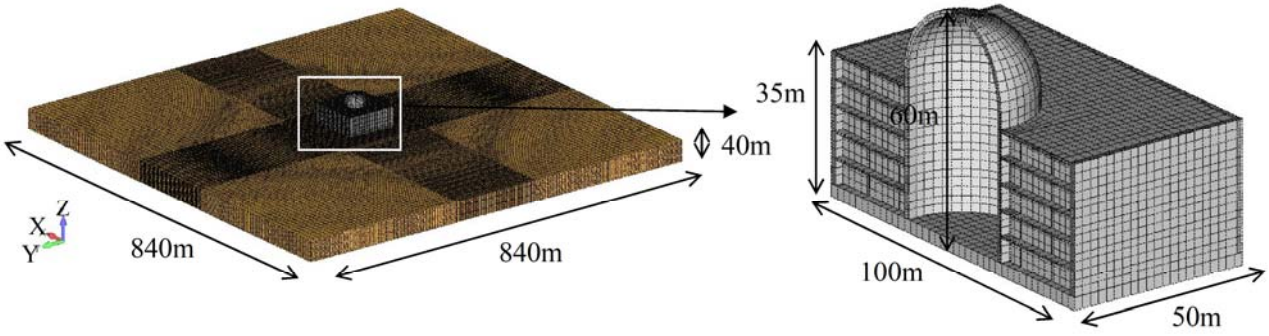

Fig. 8 – High-fidelity analysis model used to evaluate dynamic interaction effects between reactor building and soil

A viscous boundary condition was set on the bottom of the soil. The side boundary was set as traction free; the model was sufficiently large so that the effects of the traction free side boundaries on the solution became negligible. The spectrum waves proposed by Kato *et al*. [11] were used. The maximum acceleration was set 1,500 gal and the three components of the waves were input. The conditions set for the numerical analysis were summarized in Table 3. The time integration employed the Newmark-β method ($\beta = 0.25, \gamma = 0.5$). Based on the result of the eigenvalue analysis for the whole model, we set $\alpha = 1.473$ and $\beta = 0.00127$ for the structure and the soil, and $\alpha = 0$ and $\beta = 0.0001$ for the contact surface element.

Table 3 – Numerical conditions used for analysis of high fidelity model

Category	Item	Conditions for numerical analysis
Non-linear calculation	Iterative method	Newton-Raphson method
	Convergence criterion	1.0×10^{-5}
	Maximum number of iterations	50
	Dynamic step	0.001 sec/step
	Total step	22,090 (22.09 sec)
Method to solve the inverse matrix	Solver	CG method
	Precondition	Slice Successive Over Relaxation
	Convergence criterion	1.0×10^{-8}
	Maximum number of iterations	100,000
	The number of parallel	64

4.2 Comparisons of the responses

The time histories of displacements and accelerations at the top of the reactor building are shown in Fig. 9; the number of Gauss integration points of the contact surface element was 4. The maximum horizontal displacement and acceleration were 0.2 m and 2,000 gal, respectively; the acceleration becomes 1.3 times greater than the maximum input acceleration of 1,500 gal.

In comparing the response results of the contact surface element and the joint element, it is seen that both the displacement and the acceleration agree with each other. In particular, there is no significant differences in the behavior of the building due to the different elements.

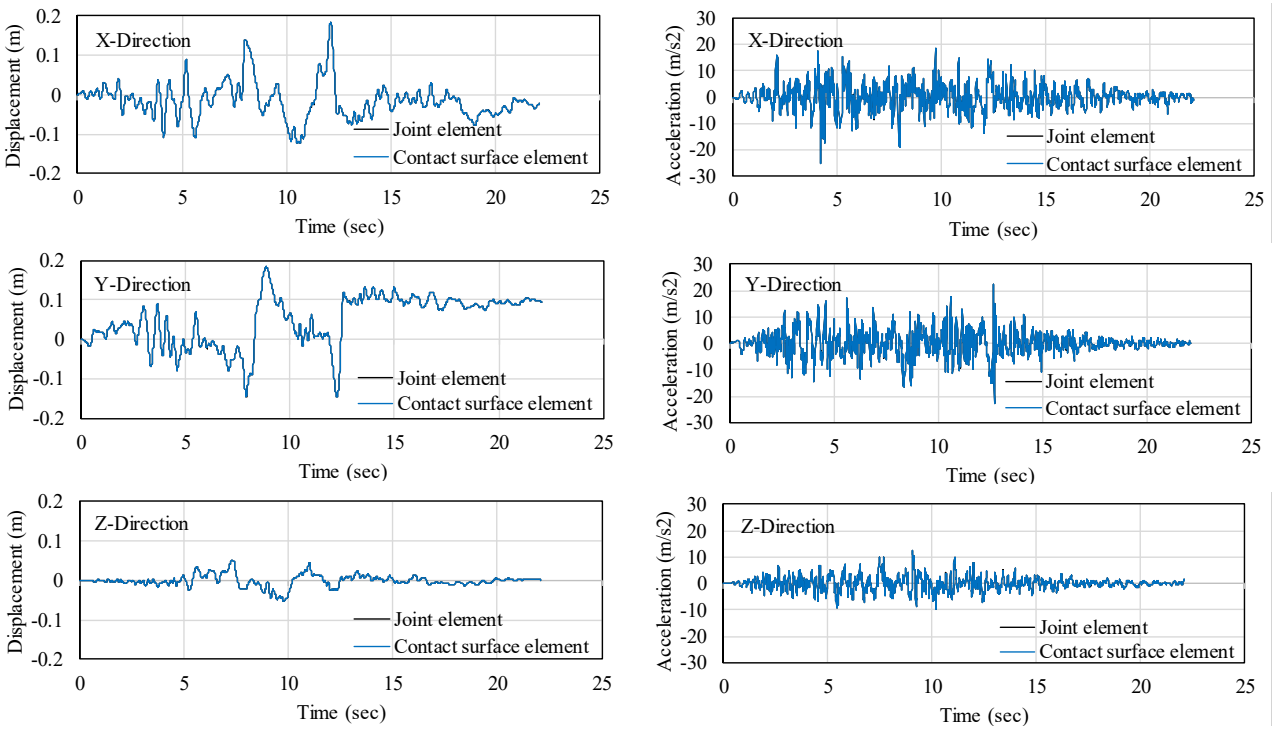

Fig. 9 – Time histories of responses at top of reactor building (left side: displacements, right side: accelerations)

Figure 10 shows the distribution of vertical stress on the contact surface at the time of 5.45 sec when the contact area between the foundation and soil is minimized. The vertical stress at the center of the element is used for the comparison of the joint element and contact force element. The average of the nodal force is used for the joint element, and the surface integral of traction is used for the contact surface element; Gauss integration points, the number of which is 36, is used for the integral. It is seen that the distribution of vertical stress is slightly different. However, both the contact surface element and the joint element have a smooth distribution of vertical stress even at the boundary between contact and separation areas.

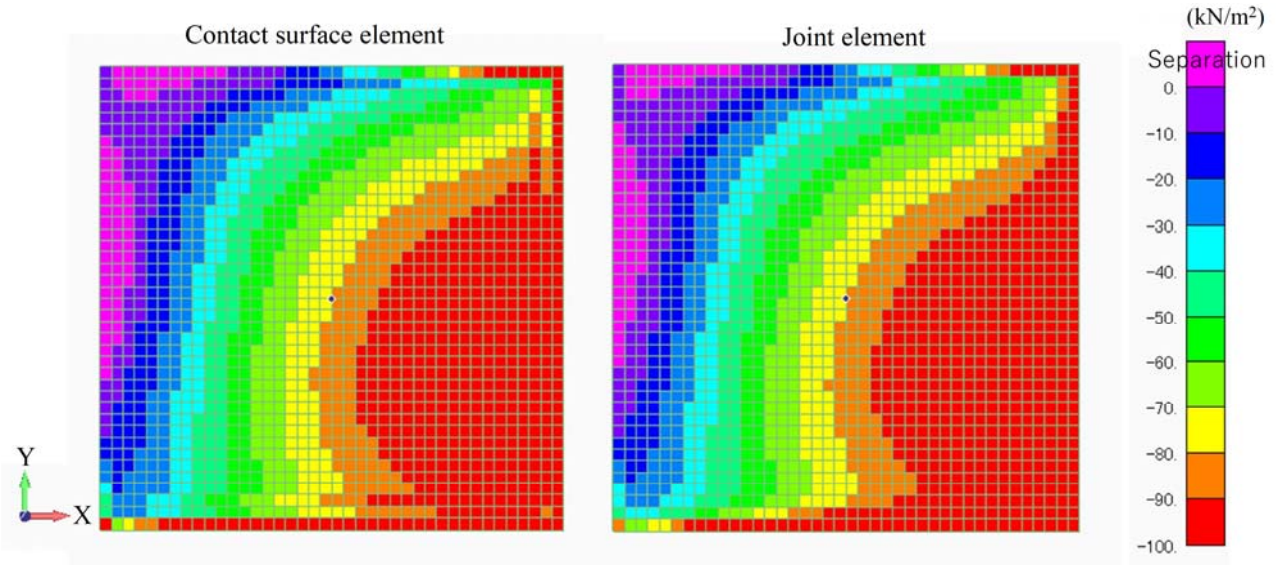

Fig. 10 – Distribution of vertical stress at center of element on contact surface during dynamic analysis

The number of iterations which are needed for the CG method to reach a numerically converged solution and the computation time are summarized in Table 4; the two models are used for the contact surface element and one model is used for the joint element. There is no significant difference in the number of iterations for the CG method for the two models which have different number of the Gauss integration points. As the number of integration points increases, the computation time increases as expected. The total number of iterations for the CG method is slightly smaller for the contact surface element compared with the joint element, and the computation time is slightly shorter, too. This result suggests the potential usefulness of the surface element, because it is more rigorous but does not increase computational cost.

Table 4 – Comparison of contact surface element and joint element in terms of number of iterations for CG method and computation time

Type	**Total number of iterations for CG method**	**Computation time (sec)**
Contact surface element: 4 integration points	5,534,597	70,000
Contact surface element: 36 integration points	5,532,163	81,927
Joint element	5,598,364	71,118

5. Conclusions

In this paper, we developed a contact surface element based on the rigorous formulation of the energy stored on the contact surface. The element was verified and implemented into HPC-FEM. It was shown that HPC-FEM was able to calculate contact and separation of a structure and ground which is induced by ground motion, if damping ratio and spring coefficients are properly chosen for the element. The potential usefulness of HPC-FEM implemented with the contact surface element was demonstrated, based on the results of the seismic response analysis of a high fidelity model of a nuclear power plant. The comparison of the joint element suggests the superiority of the contact surface element in terms of the accuracy and the computation cost.

The contact surface element has simplicity in determining spring coefficients in terms of stiffness and strength per area and flexibility in dealing with contact surfaces of heterogeneity and complex configuration. Moreover, it is able to rigorously compute partial contact and separation on a contact surface, by increasing the number of Gauss integration points. It is worth being examined to carry out more detailed numerical study on the seismic response analysis of nuclear power plant facilities which are built on heterogeneous ground, using HPC-FEM implemented with the contact surface element.

6. References

[1] Yoshimura S, Hori M, Ohsaki M (2016): *High-Performance Computing for Structural Mechanics and Earthquake/Tsunami Engineering*, Springer Tracts in Mechanical Engineering.

[2] Hotta W, Suzuki S, Hori M (2019): On Contraction of Three-Dimensional Multiple Shear Mechanism Model for Evaluation of Large Scale Liquefaction Using High Performance Computing, *Geosciences*, **9** (1).

[3] Motoyama H, Sonobe H, Hotta W, Suzuki S, Hori M (2019): Basic Study on Development and Validation of Seismic Response Analysis Using High-Fidelity Model for Large-Scale Reinforced Concrete Structures, *Journal of Japan Association for Earthquake Engineering*, **19** (5), 345-355.

[4] Goodman RE, Taylor RL, Brekke TL (1968): A model for the mechanics of jointed rocks, *Journal of the Soil Mechanics and Foundations Division, ASCE,* **94** (3), 637-659.

[5] Toki K, Miura F, Otake T (1982): NON-LINEAR SEISMIC RESPONSE ANALYSIS OF SOIL-STRUCTURE INTERACTION SYSTEM BY 3-DIMENSIONAL JOINT ELEMENT, *Proceedings of the Japan Society of Civil Engineers*, (322), 51-61.

[6] Schellekens JCJ, De Borst R (1993): On the numerical integration of interface elements, *International Journal for Numerical Methods in Engineering*, **36** (1), 43-66.

[7] Vignollet J, May S, De Borst R (2014): On the numerical integration of isogeometric interface elements, *International Journal for Numerical Methods in Engineering*, **102** (11), 1733-1749.

[8] Hori M, Oguni K, Sakaguchi H (2005): Proposal of FEM implemented with particle discretization for analysis of failure phenomena, *Journal of the Mechanics and Physics of Solids*, **53** (3), 681-703.

[9] Wijerathne MLL, Oguni K, Hori M (2009): Numerical analysis of growing crack problems using particle discretization scheme, *International Journal for Numerical Methods in Engineering*, **80** (1), 46-73.

[10] FrontISTR Forum. FrontISTR ver.4.5. Available online: http://www.multi.k.u-tokyo.ac.jp/FrontISTR/files/FISTRv4.5E.pdf (accessed on 27 December 2019).

[11] Kato K, Miyakoshi K, Takemura M, Inoue D, Ueta K, Dan K (2004): Earthquake Ground Motions by Blind Faults in the Upper Crust -Categorization of Earthquakes Based on Geological Survey and Examination of the Upper Level from Strong Motion Records-, *Journal of Japan Association for Earthquake Engineering*, **4** (4), 46-86.

